Simplistic correlations between molecular electronic properties and inhibition efficiencies

Do they really exist?

Kokalj, Anton; Lozinšek, Matic; Kapun, Barbara; Taheri, Peyman; Neupane, Shova; Losada-Pérez, Patricia; Xie, Chenyang; Stavber, Stojan; Crespo, Daniel; Renner, Frank U.

Important note
To cite this publication, please use the final published version (if applicable).
Please check the document version above.

Simplistic correlations between molecular electronic properties and inhibition efficiencies: Do they really exist?

Anton Kokalj[a],*, Matic Lozinšek[a],[1], Barbara Kapun[a], Peyman Taheri[b], Shova Neupane[c],[2], Patricia Losada-Pérez[c],[3], Chenyang Xie[d], Stojan Stavber[a], Daniel Crespo[d], Frank U. Renner[c], Arjan Mol[b], Ingrid Milošev[a]

[a] *Department of Physical and Organic Chemistry, Jožef Stefan Institute, Jamova 39, SI-1000 Ljubljana, Slovenia*
[b] *Department of Materials Science and Engineering, Delft University of Technology, 2628 CD Delft, The Netherlands*
[c] *Instituut voor Materiaalonderzoek (IMO), Universiteit Hasselt, BE-3590 Diepenbeek, Belgium*
[d] *Universitat Politècnica de Catalunya/BarcelonaTech, Departament de Física, INTE, Barcelona Res. Center in Multiscale Sci. & Tech., 08930 Barcelona, Spain*

ABSTRACT

The often used simplistic correlations between molecular electronic parameters and experimentally determined corrosion inhibition efficiencies are critically evaluated for a set of 24 heterocyclic organic compounds, tested as corrosion inhibitors for copper in 3 wt.% NaCl aqueous solution. Twelve different molecular electronic descriptors—such as ionization potential, electron affinity, HOMO–LUMO gap, dipole moment—are tested and it is shown that none of them displays any noticeable correlation with the inhibition efficiency. Our results, therefore, cast serious doubt on reported correlations between such parameters and inhibition efficiency, obtained for only a few inhibitors, which are abundant in the literature. We also discuss some pros and cons of inhibition efficiency as a metric for evaluating the performance of corrosion inhibitors, and introduce a new metric termed *inhibition power* that uses the universal logarithmic scale and dimensionless decibel (dB) units.

1. Introduction

Corrosion inhibitors are substances, used in relatively low concentrations, that effectively reduce the rate of corrosion of metals and their alloys. They are used in various applications such as cooling systems, storage tanks, boilers, oil pipelines, oil well drilling technology, architecture, and cultural heritage, to name a few.

The use of corrosion inhibitors to mitigate corrosion has proven to be an efficient and simple mode of protection, provided that the right inhibitor substance is used for a given application (note that the efficiency of a given corrosion inhibitor depends on the metallic material and the environment to which the material is exposed). Due to complexity of corrosion inhibition, good inhibitors have been, in most cases, determined in a purely empirical manner out of large sets of organic compounds, where experimental testing provided information on whether a specific compound is effective for a given substrate in a given medium. The current state-of-the-art in this field is therefore represented by high-throughput experimental testing [1–7]. In contrast to

such empirical trial-and-error approaches, rational design of new corrosion inhibitors with potentially superior corrosion inhibition characteristics would represent a major breakthrough in the field of corrosion prevention [8,9]. To this end, molecular modeling of corrosion inhibitors has become fashionable [10–13], although cases where new efficient inhibitors have been suggested on the basis of molecular modeling studies are rare. Among various approaches, machine-learning techniques currently have the largest potential to generate reasonably robust and predictive models for screening new inhibitors, however, the number of such studies is not large (see, e.g., Refs. [3,14,9,15–21] and the review of Winkler [22]). Instead, the large majority of molecular modeling studies of corrosion inhibitors relies on calculating several molecular electronic properties and associating them to the experimentally determined corrosion inhibition efficiency (IE) via some correlation analysis, which in most cases is a simplistic linear correlation between a given molecular parameter and IE. This approach was named MEPTIC in Ref. [12]; the acronym stands for Molecular-Electronic Properties To Inhibition-efficiency Correlation.

Among the most popular parameters in the MEPTIC approach are eigenvalues of the highest occupied (HOMO) and lowest unoccupied (LUMO) molecular orbitals, HOMO–LUMO gap, electronegativity, chemical hardness, dipole moment, Fukui indices, etc. The MEPTIC approach is based on two premises. The first is that these molecular parameters are important reactivity indicators that can reasonably predict the trend of adsorption bonding of inhibitors. In particular, it is often argued that the higher the eigenvalue of HOMO (ε_{HOMO}) is, the larger the molecular electron donation to the metal substrate will be and the lower the eigenvalue of LUMO (ε_{LUMO}) is, the larger the electron back-donation from surface states to the molecule will be; but high ε_{HOMO} and low ε_{LUMO} implies a small HOMO–LUMO gap, because $\varepsilon_{LUMO} > \varepsilon_{HOMO}$. Hence, the smaller the HOMO–LUMO gap, the stronger the molecule–surface bonding should be. The second premise of MEPTIC is that the stronger the inhibitor binds to the surface the better (more efficient) it is. This premise originates from the observation that under simplified assumptions the inhibition efficiency can be shown to be synonymous with molecular surface coverage [23]. Many correlations between these parameters and IE were claimed to be established in the literature, however, many of these are based only on a few inhibitors (often only two or three). These are therefore susceptible to chance correlation and even more so to spurious correlation fallacy, because correlation does not imply causation. Such an approach was criticized, e.g., by Kokalj et al. [24,25] on conceptual grounds and by Winkler et al. [3,14] on statistical grounds, who demonstrated that for a large dataset of corrosion inhibitors the correlation between inhibitor's frontier orbital parameters and inhibitor efficiency for aluminum alloys AA2024 and AA7075 disappears.

The purpose of this study is to specifically evaluate simplistic linear correlations between 12 different molecular electronic parameters and IE for a moderately large set of heterocyclic compounds for copper in 3 wt.% aqueous NaCl solution. The set consists of 26 different organic heterocyclic compounds, shown in Fig. 1, out of which 23 belong to azole family. These molecules are on the one hand sufficiently versatile (they are not homologous) and on the other hand sufficiently similar to make the MEPTIC approach viable. Namely, the MEPTIC approach is not expected to work for sufficiently dissimilar molecules. We will show that none of the 12 evaluated parameters correlates with experimentally measured IE. While this is a negative result, we believe it is important, because the literature is replete with studies, based on only a few inhibitors, where purported correlations between such parameters and IE are claimed. In contrast, our study provides strong support to the statement made by Lindsay et al. [26] several years ago that *"In terms of predictive power, such an approach has at best limited value, and is potentially simply misleading"* with emphasis on the last part of the sentence.

2. Technical details

2.1. Inhibitors

24 different organic heterocyclic compounds, mainly from the azole family, were tested as corrosion inhibitors (actually the whole set comprises 26 molecules, but the measurements could not be reliably performed for two compounds due to their too low solubility). Their skeletal formulae as well as shorthand labels are shown in Fig. 1. Nomenclature of the labels follows these four rules:

1. Labels of the common parent compounds are: imidazole (ImiH), benzimidazole (BimH), and benzotriazole (BTAH). Labels for other parent compounds are: indazole (InzH), indole (IndH), quinoline (Quin), and benzothiophene (Btp).
2. A functional group attached either to azole or heterocycle ring prefixes the parent label (e.g., SH-BimH stands for mercaptobenzimidazole).
3. A functional group attached to the fused benzene ring suffixes the

parent label (e.g., BimH-5OMe stands for 5-methoxybenzimidazole)
4. A methyl (Me), propyl (Pr), butyl (Bu), octyl (Oc), or decyl (De) group attached to the azole N1 atom suffixes the parent label such that the trailing H is substituted by the group acronym (e.g., ImiMe stands for 1-methylimidazole).

To facilitate the presentation, inhibitors are divided into four groups (Fig. 1) according to their chemical nature, in particular: (1) azoles that contain a thiol SH group (mercapto-azoles); (2) heterocycles containing an OH group (hydroxy-heterocycles); (3) benzazoles; and (4) imidazole derivatives. Among these heterocycles only three from the group-2 do not belong to the azole family; these are 7-hydroxyindole, 8-hydroxyquinoline, and benzothiophene-2-methanol.

Group-1 contains 8 mercapto-azoles, two imidazoles and six benzimidazoles. Following the order from Fig. 1, these are: 2-mercapto-1-methylimidazole (SH-ImiMe), 2-mercapto-4-phenylimidazole (SH-ImiH-4Ph), 2-mercaptobenzimidazole (SH-BimH), 2-mercapto-1-methylbenzimidazole (SH-BimMe), 2-(methylthio)benzimidazole (Me-S-BimH), 2-mercaptomethyl benzimidazole (SH-Me-BimH),[4] 2-mercapto-5-methoxybenzimidazole (SH-BimH-5OMe), 5-amino-2-mercaptobenzimidazole (SH-BimH-5NH$_2$).

Group-2 contains 5 hydroxy-heterocycles: 2-hydroxybenzimidazole (OH-BimH), benzimidazole-2-methanol (OH-Me-BimH), 7-hydroxyindole (IndH-7OH), 8-hydroxyquinoline (Quin-8OH), benzothiophene-2-methanol (OH-Me-Btp). Note that the last three, though heterocycles, are not azoles.

Group-3 contains 7 compounds: indazole (InzH), three benzimidazoles—benzimidazole (BimH), 1-methylbenzimidazole (BimMe), 5-methoxybenzimidazole (BimH-5OMe)—and three benzotriazoles—benzotriazole (BTAH), 1-methylbenzotriazole (BTAMe), 1H-benzotriazole-6-carboxylic acid (BTAH-6COOH).

Group-4 contains 6 imidazole derivatives: imidazole (ImiH), 1-butylimidazole (ImiBu), 1-(3-aminopropyl)imidazole (ImiPrNH$_2$), 1-(3-hydroxypropyl)imidazole (ImiPrOH), 1-octylimidazole (ImiOc), 1-decyl-2-methylimidazole (Me-ImiDe).

These compounds were purchased from Fluorochem (Me-S-BimH (95%), SH-Me-BimH·HCl (95%), SH-BimH-5OMe (95%), SH-BimH-5NH$_2$ (97%); OH-BimH (97%), OH-Me-BimH (97%), IndH-7OH (95%), Quin-8OH (98%), OH-Me-Btp (97%); InzH (98%), BimMe (95%), BimH-5OMe (95%), BTAMe (98%), BTAH-6COOH (95%); ImiBu (99%), ImiPrNH$_2$ (98%), ImiPrOH (>98%), ImiOc (95%)), Sigma-Aldrich (SH-ImiMe (99 + %), SH-ImiH-4Ph (97%), SH-BimH (98%), SH-BimMe (95%), BimH (98%), ImiH (99.5%), Me-ImiDe (97%)), and Fluka (BTAH (99%)).

2.2. Computational

DFT calculations were performed with the `Gaussian16` program [27] using the hybrid B3LYP functional [28], which is known to be reasonably accurate for the description of organic molecules [29]. Electrons were described with local Gaussian-type orbital basis set, in particular with Def2-TZVP [30], which is an all electron triple-ζ basis set with polarization functions. Convergence tests reveal that this basis set gives reasonably converged electronic properties. Calculations were performed for standalone molecules in vacuum and in implicit aqueous solvent, described with the SMD solvent model [31]. Unless explicitly stated otherwise, reported molecular electronic parameters refer to standalone molecules in vacuum.

In this manuscript we focus on twelve global molecular electronic

---

[4] Note that this compound was purchased as 2-mercaptomethyl benzimidazole hydrochloride (SH-Me-BimH·HCl), however, we will exclusively refer to mercapto compound itself and use the SH-Me-BimH label. Such simplification seems reasonable, because it can be inferred that it is only the SH-Me-BimH compound that is responsible for corrosion inhibition.
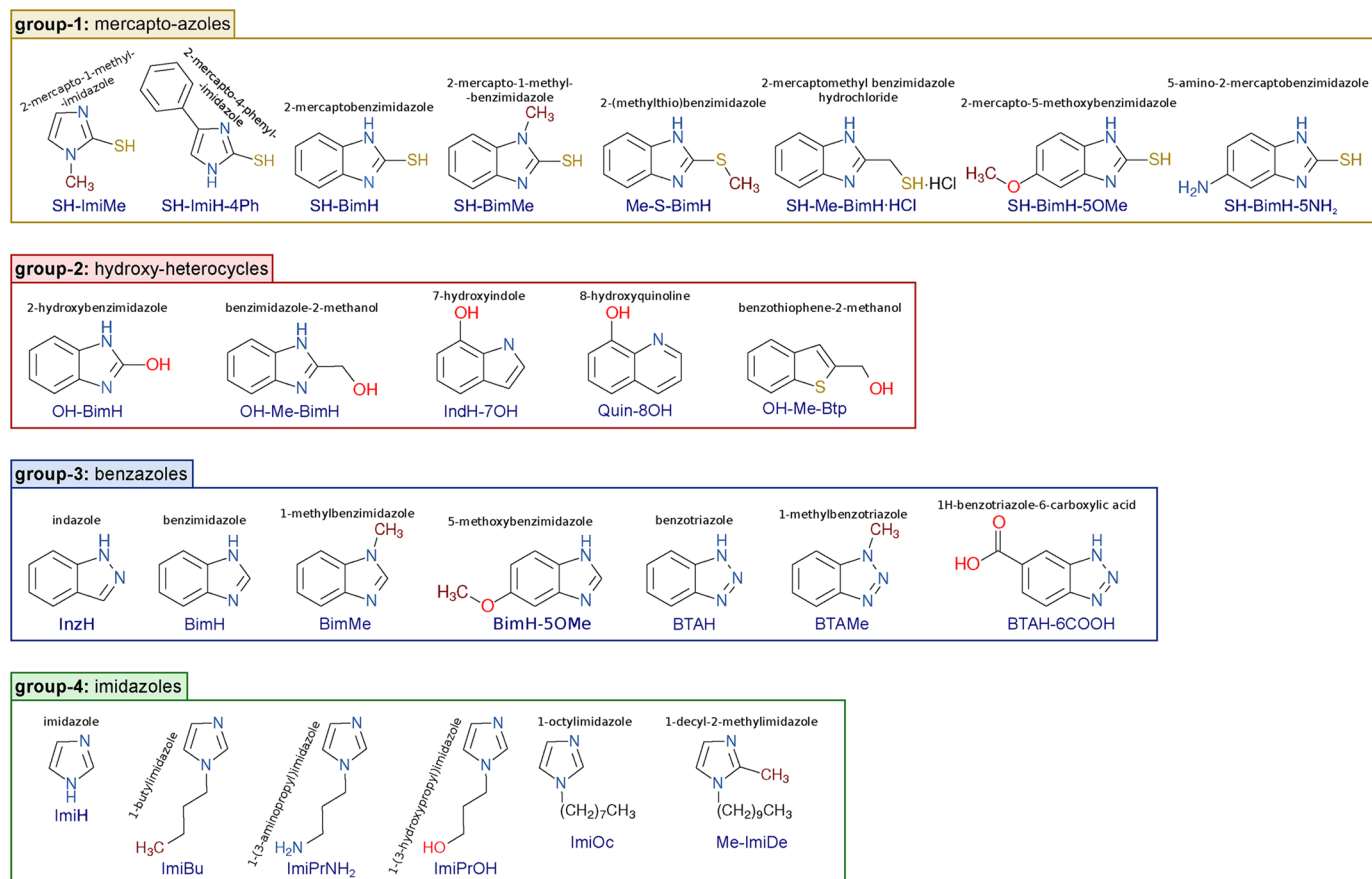
Fig. 1. Twenty-six heterocyclic organic compounds—23 of them belong to the azole family—considered in this work along with the definition of their shorthand labels. Compounds are divided into four chemical groups: (1) molecules containing an SH group (mercapto-azoles), (2) molecules containing an OH group (hydroxy-heterocycles), (3) benzazoles, and (4) imidazole derivatives. For two hydroxy-heterocycles (IndH-7OH and OH-Me-Btp) the measurements could not be reliably performed due to their too low solubility.

parameters that are often used in the MEPTIC approach, in particular: vertical ionization potential and electron affinity, chemical hardness, electronegativity, HOMO and LUMO eigenvalues, HOMO–LUMO gap, polarizability, dipole moment, HSAB (hard and soft acids and bases) ΔN and ΔE parameters, and electrophilicity (in the Supplementary material, we also consider molecular solvation energies). Several of these parameters originate from a theoretical formalization [32] of the HSAB principle [33], which is based on the first and second partial derivatives of energy E with respect to electron number N at constant external potential v:

$$\mu = \left(\frac{\partial E}{\partial N}\right)_v \quad \text{and} \quad \eta = \frac{1}{2}\left(\frac{\partial^2 E}{\partial N^2}\right)_v, \tag{1}$$

where μ and η are the electron chemical potential and the absolute chemical hardness, respectively. However, these derivatives are ill defined due to integer discontinuities [34]. A way out is to assume a continuous $E(N)$ curve, such as the ground-state parabola model [35] which gives:

$$\chi = \frac{I + A}{2} = -\mu, \tag{2}$$

$$\eta = \frac{I - A}{2}, \tag{3}$$

where χ is the Mulliken electronegativity [36,37]. I and A are the vertical ionization potential (IP) and vertical electron affinity (EA), respectively, defined as:

$$I = [E_{X^+} - E_X]_v, \tag{4}$$

$$A = [E_X - E_{X^-}]_v, \tag{5}$$

where X stands for the neutral molecule, while X^+ and X^- are the corresponding cation and anion, respectively ($X^+ + e^- \to X$ and $X + e^- \to X^-$), with the molecular geometries constrained to that of X.

Three calculations are therefore required to calculate IP and EA. For this reason IP is often approximated by the eigenvalue of the HOMO orbital ($I \approx -\varepsilon_{\text{HOMO}}$) and EA by the eigenvalue of the LUMO orbital ($A \approx -\varepsilon_{\text{LUMO}}$). We instead calculated IP and EA explicitly with Eqs. (4) and (5), respectively, and treated $\varepsilon_{\text{HOMO}}$ and $\varepsilon_{\text{LUMO}}$ as separate parameters.

The HOMO–LUMO gap is another popular parameter in MEPTIC studies. It is defined as:

$$\Delta\varepsilon = \varepsilon_{\text{LUMO}} - \varepsilon_{\text{HOMO}}. \tag{6}$$

Note that within the "HOMO–LUMO approximation" the HOMO–LUMO gap is proportional to the chemical hardness, i.e., $\eta \approx 2\Delta\varepsilon$. Furthermore, a factor $1/2$ is often omitted [38] in the definition of chemical hardness (cf. Eq. (1)) so that $\eta = \left(\frac{\partial^2 E}{\partial N^2}\right)_v$. In this case the HOMO–LUMO gap becomes synonymous with chemical hardness, $\eta \approx \Delta\varepsilon$.

Two further important HSAB-based parameters are the electron charge transfer (ΔN) from Lewis base B to Lewis acid A and the associated change in energy (ΔE) which are defined as [32]:

$$\Delta N = \frac{\chi_A - \chi_B}{2(\eta_A + \eta_B)}, \tag{7}$$

and

$$\Delta E = -\frac{(\chi_A - \chi_B)^2}{4(\eta_A + \eta_B)}, \tag{8}$$

where $\Delta N \equiv \Delta N_A = -\Delta N_B$ measures the charge transferred from B to A. In the case of interaction of a molecule with a metal surface, the ΔN and ΔE equations can be written as (A = metal, B = mol, and $\eta_{metal} \approx 0$):

$$\Delta N = \frac{\chi_{metal} - \chi_{mol}}{2(\eta_{metal} + \eta_{mol})} = \frac{\Phi - \chi_{mol}}{2\eta_{mol}}, \tag{9}$$

and

$$\Delta E = -\frac{(\chi_{metal} - \chi_{mol})^2}{4(\eta_{metal} + \eta_{mol})} = -\frac{(\Phi - \chi_{mol})^2}{4\eta_{mol}}, \tag{10}$$

where the calculated work function (Φ) of Cu(111) of 4.83 eV was used for the electronegativity of copper surface [39].

Another widely used parameter related to ΔE is the electrophilicity index (ω) [40] defined as:

$$\omega = \frac{\chi^2}{4\eta}. \tag{11}$$

Note that the original definition of the electrophilicity index is $\omega = \frac{\mu^2}{2\eta}$, however, Parr et al. [40] omitted the factor 1/2 in the definition of η, i.e., $\eta = \partial^2 E / \partial N^2$. Hence, Eq. (11) is consistent with η defined by Eq. (1) [41].

The last two molecular electronic parameters that we utilized are the isotropic polarizability (α) and the molecular dipole ($\boldsymbol{p}$), which are related to one another as:

$$\boldsymbol{p} = \boldsymbol{p}_0 + \alpha \boldsymbol{E}, \tag{12}$$

where $\boldsymbol{p}_0$ is the zero-field dipole and $\boldsymbol{E}$ is external electric field. Polarizability therefore measures a linear response of a molecular charge distribution to external electric field. We considered only the magnitude of the dipole as a MEPTIC parameter, $p_0 = |\boldsymbol{p}_0|$.

2.3. Experimental

Corrosion tests were performed on copper metal (99.9%), purchased from Goodfellow (Cambridge Ltd., UK) in the form of a 2 mm thick sheet. Specimens were first cut from the sheet in the shape of discs of 15 mm diameter and then mechanically ground, on a rotating plate polisher, under a stream of water, using SiC papers of progressively finer gradations from 500 to 800, 1000, 1200, 2400, and finally 4000. Copper samples were then cleaned with ethanol in an ultrasonic bath for three minutes, rinsed twice with distilled water, and dried with nitrogen gas.

Samples were immersed in 3 wt.% aqueous NaCl solutions with or without the inhibitor in 1 mM concentration. As a method for evaluating the performance of compounds as corrosion inhibitors, we chose linear polarization resistance, measured at discrete times over a 100 h time interval [42], as described below. Each measurement was repeated at least three times.

2.3.1. Linear polarization resistance measurements

Electrochemical measurements were performed in a three-electrode corrosion cell (volume 0.25 L, Autolab, Ecochemie, Netherlands) at 25 °C. Either a saturated calomel electrode (SCE, 0.242 V with respect to the standard hydrogen electrode (SHE) at 25 °C) or an Ag|AgCl‖3M KCl electrode (0.207 V with respect to SHE at 25 °C) with a Luggin capillary was used as a reference electrode. Carbon rods were used as the counter electrode. A specimen embedded in a Teflon holder, with an area of 0.785 cm^2 exposed to the solution, served as the working electrode.

Linear polarization resistance (LPR or R_p) measurements were executed with a multichannel potentiostat/galvanostat Autolab Model M204 (Metrohm Autolab, Utrecht, Netherlands) operated by the NOVA

software. Each measurement lasted for 100 h. At discrete times of 1, 2, 3, 5, 24, 48, 72, and 100 h the LPR was measured over a potential range of ± 10 mV vs. corrosion potential using a scan rate of 0.1 mV/s. The R_p values were obtained from the slope of the fitted potential vs. the current density using the NOVA software.

Measurements were repeated at least three times for each inhibitor and at each discrete time t_k the $R_p(t_k)$ was averaged as:

$$\langle R_p(t_k) \rangle = \frac{1}{m} \sum_i^m R_p^{(i)}(t_k), \tag{13}$$

where m is the number of measurements and $R_p^{(i)}(t_k)$ is the value of R_p at discrete time t_k at the ith measurement. The mean value of R_p over a 100 h interval was then calculated via trapezoidal integration as:

$$R_p \equiv \overline{R_p} = \frac{1}{t_M - t_1} \int_{t_1}^{t_M} \langle R_p(t) \rangle \, dt$$

$$\approx \frac{1}{t_M - t_1} \sum_{k=2}^{M} \frac{\langle R_p(t_{k-1}) \rangle + \langle R_p(t_k) \rangle}{2} \Delta t_k \tag{14}$$

and

$$\Delta t_k = t_k - t_{k-1},$$

where M is the number of discrete times at which R_p was measured. For the sake of brevity we will often designate $\overline{R_p}$ simply as R_p as suggested by $R_p \equiv \overline{R_p}$ equivalence in the equation. Finally, the inhibition efficiency (IE or η) was calculated as:

$$\eta = \frac{R_p^{inh} - R_p^{blank}}{R_p^{inh}}, \tag{15}$$

where R_p stands for $\overline{R_p}$ as defined by Eq. (14), R_p^{inh} is the mean polarization resistance of the inhibited sample and R_p^{blank} is the mean value of the blank non-inhibited sample. Note that the symbol η used for IE coincides with that used for chemical hardness, Eq. (3). The reason that we use the symbol η despite this inconvenience is because it is commonly used for IE in the literature. However, we believe it will be clear from the context which property is meant when the symbol η is used.

3. Results and discussion

3.1. Pros and cons of IE metric

IE as a measure of the performance of the inhibitor has some pros and cons. Pros are: (i) it is normalized, i.e., for inhibitors $\eta \in [0, 1]$ (or
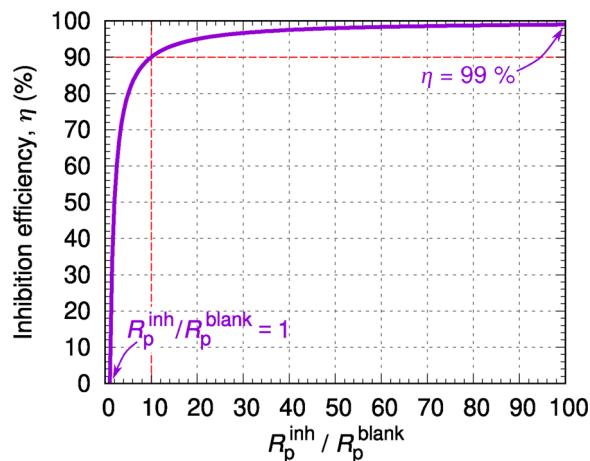

Fig. 2. Dependence of the inhibition efficiency on R_p^{inh}. This dependence is highly nonlinear, i.e., at low values of R_p^{inh} the IE increases very rapidly for a small increase of R_p^{inh}, whereas for IE $\gtrsim 90\%$ it increases very slowly for a large increase of R_p^{inh}.
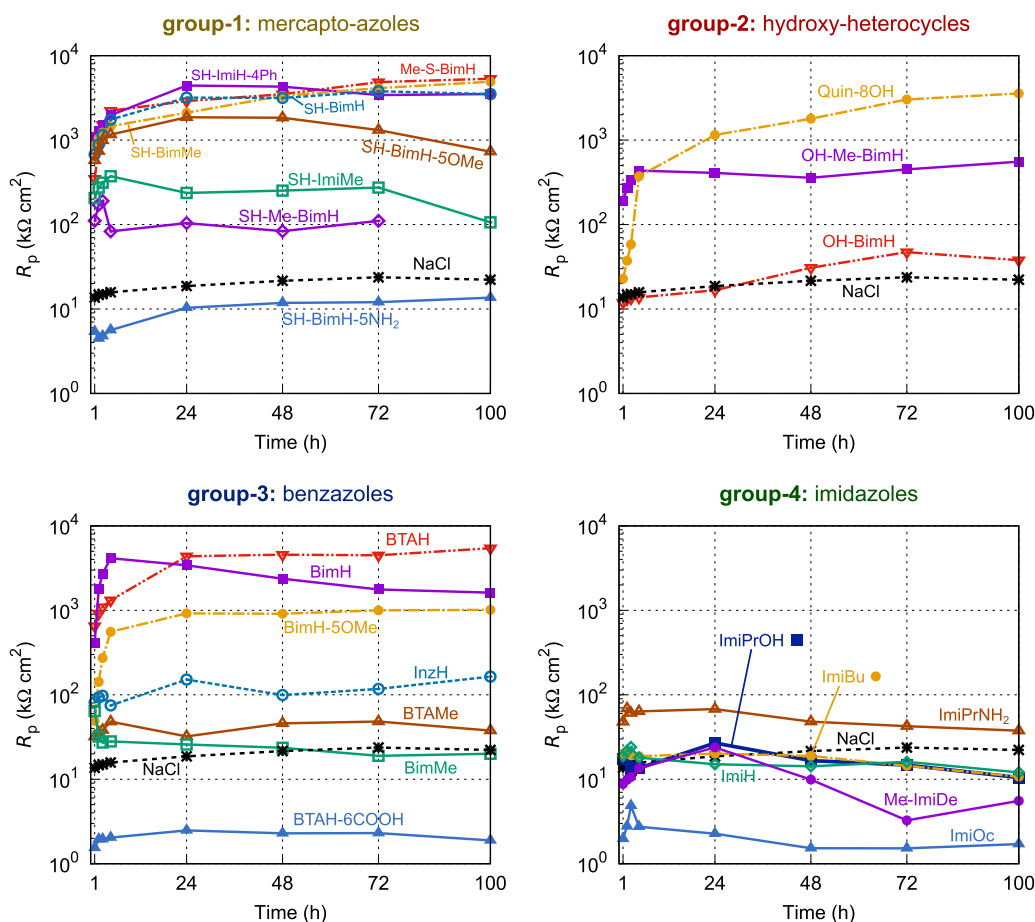
Fig. 3. Average linear polarization resistance, R_p, measured at discrete times (points) over a 100 h interval for copper in a 3 wt.% NaCl solution with and without addition of 1 mM of inhibitor for all four groups of inhibitors as listed in Fig. 1; note the logarithmic scale of R_p. Each point is the average R_p value at a particular discrete time obtained from at least three measurements, i.e., it corresponds to $\langle R_p^{inh}(t_k)\rangle$ of Eq. (13).

between 0 and 100%), although for corrosion activators it becomes negative; (ii) it can be shown under simplifying assumptions that η is synonymous with molecular surface coverage θ, $\eta \approx \theta$. However, the drawback of IE is that it is highly nonlinear. This nonlinearity can be appreciated from Fig. 2, which plots IE as a function of R_p^{inh}/R_p^{blank} ratio. It is evident that at low values of R_p^{inh} the IE increases very rapidly for a small increase of R_p^{inh}, whereas for IE $\gtrsim$ 90% it increases very slowly for a large increase of R_p^{inh}. Hence, for $\eta \gtrsim 90\%$ a small increase of IE indicates significant reduction of corrosion, whereas for small values of η (say below about 50%) a large increase of IE indicates only small reduction of corrosion. Due to this nonlinearity it is difficult to differentiate very good inhibitors by IE, as will become evident below. For this reason, we will introduce below a new metric termed *inhibition power* that uses the logarithmic scale and dimensionless decibel (dB) units.

3.2. Experimental results

Fig. 3 plots LPR as a function of time for copper samples, measured at discrete times over 100 h interval in 3 wt.% NaCl solution with and without 1 mM inhibitor for all four groups of inhibitors (one plot per each group). The mean value of R_p for a blank sample (labeled as NaCl) over a 100 h period is about 20 kΩ cm^2. The following observations are evident from the figure:

(i) Five compounds from group-1 (mercapto-azoles) perform as good inhibitors (Me-S-BimH, SH-ImiH-4Ph, SH-BimMe, SH-BimH, and

SH-BimH-5OMe) with $\langle R_p^{inh}(t_k)\rangle$ values above about 10^3 kΩ cm^2. Two compounds (SH-ImiMe and SH-Me-BimH) perform moderately with $\langle R_p^{inh}(t_k)\rangle$ values above about 10^2 kΩ cm^2, whereas SH-BimH-5NH$_2$ acts as a corrosion activator. It should be noted that the SH-Me-BimH·HCl compound is apparently unstable in the NaCl solution; it seems that SH-Me-BimH decomposes (the solution becomes colored yellow after about two days),[5] which is why the measurements were terminated prematurely.

(ii) As for group-2 (hydroxy-heterocycles), the measurements could not be reliably performed for IndH-7OH and OH-Me-Btp compounds due to their too low solubility, hence the $\langle R_p^{inh}(t_k)\rangle$ values for only three compounds are reported. The most efficient among them appears to be Quin-8OH, with $\langle R_p^{inh}(t_k)\rangle$ values above 10^3 kΩ cm^2 for $t > 24$ h, but it should be noted that during the measurements a slime-like layer appeared on the sample. OH-Me-BimH also performs moderately well, whereas OH-BimH is a weak inhibitor.

(iii) Three compounds from group-3 (benzazoles) display $\langle R_p^{inh}(t_k)\rangle$ values at about or above 10^3 kΩ cm^2 (BTAH, BimH, BimH-5OMe), followed by InzH and BTAMe with moderate values of $\langle R_p^{inh}(t_k)\rangle$. The effect of BimMe on R_p is weak, whereas BTAH-6COOH is a corrosion activator.

(iv) Compounds from group-4 (imidazoles) perform the worst. Only

---

[5] If the solution is prepared by neutralization of HCl from SH-Me-BimH·HCl by NaOH, then the resulting solution appears to be even less stable, because white fiber-like precipitates form after about 15 h.
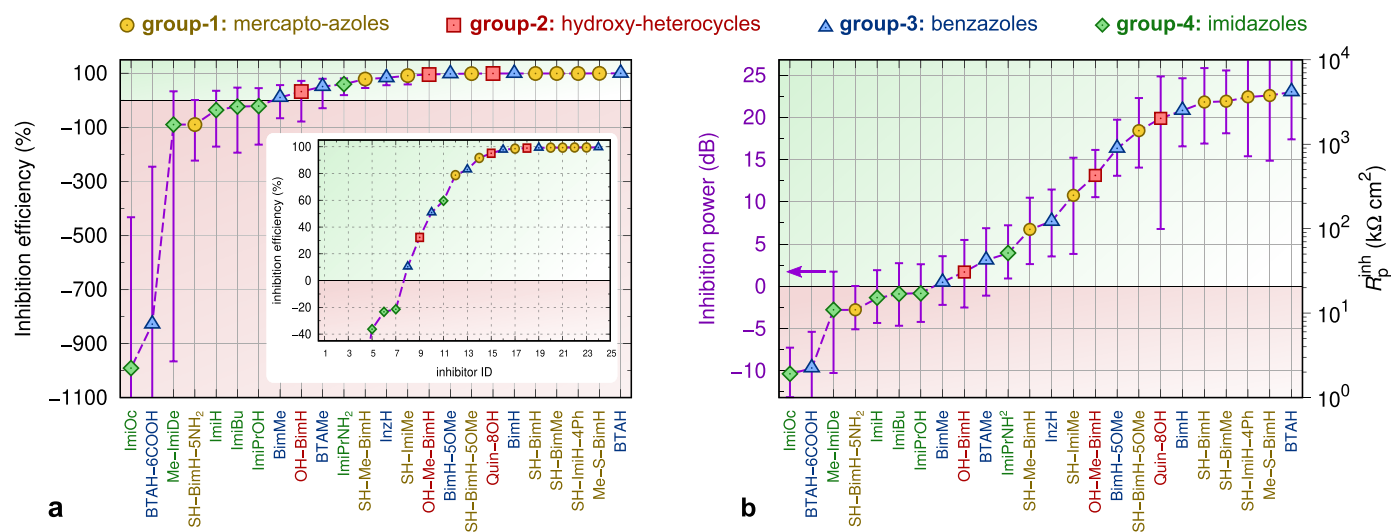
Fig. 4. (a) Inhibition efficiencies, calculated with aid of Eq. (15), for the considered compounds sorted in ascending order of IE; seven compounds act as corrosion activators. It is not possible to differentiate the best inhibitors even from the inset, where the range of IE is narrowed. (b) In contrast to IE plot, the differences are easily discernible if the inhibition power, $P_{inh} = 10\log_{10}(R_p^{inh}/R_p^{blank})$, is plotted instead; note the right ordinate axis, which shows the "absolute" polarization resistance, R_p^{inh}. Data points are color symbolized according to the four groups of inhibitors as indicated by the legend at the top. Curves are drawn solely to guide the eye. IE and P_{inh} values (with error bars) are also tabulated in Table S1 in the Supplementary material. The shown error bars are estimated with Eqs. (S8) and (S12), respectively, and in (b) they refer only to P_{inh} (left ordinate axis, indicated by purple arrow). (For interpretation of the references to color in this figure legend, the reader is referred to the web version of this article.)

ImiPrNH$_2$ displays R_p values above that of the blank sample, whereas the values of all the others are below that of the blank sample.

Fig. 4a shows the IE values for the 24 compounds, which are sorted in ascending order of their IE; the data points are color symbolized such that the four groups of inhibitors can be differentiated. As mentioned above, the measurements could not be performed reliably for 2 hydroxy-compounds (7-hydroxyindole and benzothiophene-2-methanol) due to their too low solubility, hence they are excluded in the following. The plotted IE values were obtained on the basis of LPR measurements (Fig. 3) by utilizing Eqs. (13)–(15). Out of these 24 compounds, 7 act as corrosion activators. The best inhibitor according to the IE metric is BTAH and, interestingly, among the worst performers is its derivative, BTAH-6COOH. The other high performance inhibitors are several mercapto-azoles—i.e., Me-S-BimH, SH-ImiH-4Ph, SH-BimMe, SH-BimH—and benzimidazole (BimH). From Fig. 4a (even from the zoomed-in inset) the best eight or so inhibitors cannot be visually differentiated in terms of IE, because all of their values appear at 100% efficiency. This is due to the aforementioned nonlinearity of IE (cf. Fig. 2). Another drawback of this nonlinearity is that the error bars are very large for negative and low values of IE, whereas for high IE values the error bars are smaller than the symbols of the shown data points. If instead of IE, we choose as a new metric to evaluate the performance of inhibitors a quantity termed *inhibition power* (P_{inh}), expressed in dimensionless units of decibels (dB),[6] defined as:

$$P_{inh} = 10\log_{10}(R_p^{inh}/R_p^{blank}), \quad (16)$$

then the performance of inhibitors can be easily differentiated (Fig. 4b) and also the magnitudes of the error bars appear more or less independent on the inhibitor's performance. Note that a definition of this type is common in many fields of science, such as acoustics or signal processing. In these fields the power is referred to in terms of "gain" or "loss". Accordingly, an inhibitor showing a gain of 10 (20) dB increases
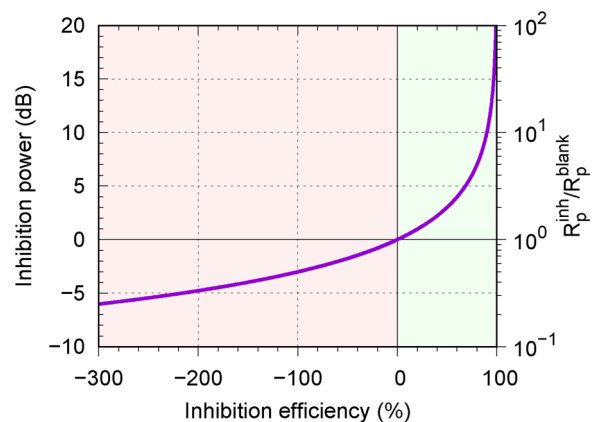

Fig. 5. Inhibition power, $P_{inh} = 10\log_{10}(R_p^{inh}/R_p^{blank})$, as a function of inhibition efficiency. Note the right ordinate axis, which shows the R_p^{inh}/R_p^{blank} ratio in logarithmic scale: it is clearly evident that the gain (loss) of 10 dB corresponds to ten fold increase (decrease) of R_p^{inh}.

the polarization resistance by a factor of 10 (100) with respect to blank solution, whereas a loss of 10 dB corresponds to a tenfold decrease of the polarization resistance; this "gain and loss" can be appreciated from Fig. 5 by comparing the left and right ordinate axes that correspond to P_{inh} and R_p^{inh}/R_p^{blank}, respectively. This figure shows the functional dependence between P_{inh} and IE and clearly reveals that IE is better suited for the evaluation of corrosion activators and "bad" inhibitors than for efficient inhibitors, whereas P_{inh} ranks compounds in an unbiased way, irrespective of their performance. Another useful property of *inhibition power* is that it can be easily associated with the corrosion rate in a P_{inh} graph, such as Fig. 4b: note that the right ordinate axis displays the "absolute" polarization resistance, although it could equally well display the corrosion rate. The reason that this axis shows R_p is due to the use of the LPR method. But P_{inh} can also be defined in terms of the corrosion rate (r), i.e., $P_{inh} = 10\log_{10}(r_{blank}/r_{inh}) = C - 10\log_{10}(r_{inh})$, where C is a constant. This implies that P_{inh} is proportional to $-\log_{10}(r_{inh})$. Hence, P_{inh} and the corrosion rate can be plotted simultaneously, the only difference with respect to Fig. 4b is that low

---

[6] Decibel (dB), as a dimensionless unit, "works" similar as percent (%) that is also dimensionless, with the difference that dB is logarithmic, whereas % is linear.

values of inhibition power correspond to high corrosion rates (i.e. the axis runs from a high to a low corrosion rate).

Returning to inhibition performance of the compounds tested in this study, the P_{inh} plot of Fig. 4b reveals—in contrast to the IE plot (Fig. 4a)—a roughly uniform distribution of inhibitor's performance from corrosion activators to very efficient inhibitors and such a wide span is particularly suitable for the MEPTIC correlation analysis.

The IE plot of Fig. 4a suggests that ImiOc and BTAH-6COOH, with IE values of around, −900% accelerate corrosion to a much larger extent than the best inhibitors are able to inhibit it; notice that the plot is dominated by the negative range of IE values, which is why the zoom-in inset is also provided. This is again the artifact of the nonlinearity of IE. In contrast, the P_{inh} plot of Fig. 4b clearly shows that this is not the case, because the ImiOc and BTAH-6COOH show a loss of 10 dB in inhibition power and therefore accelerate corrosion by a factor of 10, whereas BTAH, with the gain of 23 dB in inhibition power, reduces the rate of corrosion by as much as a factor of 200.

3.3. Computational results

Before entering into the presentation and discussion of linear correlations between experimentally determined inhibition efficiencies and computed molecular electronic properties, let us mention that most of the considered mercapto-azoles can exist in two tautomeric forms, i.e., thiol (R–SH) and thione (R=S). The transformation from thiol to thione involves the shift of H from the thiol group to the N3 atom of the azole ring and the concomitant shift of the double bond from C=N to C=S. For all currently considered molecules that can exist in the two tautomeric forms, thiones are found, in accordance with the literature [43–46], to be more stable than thiols by about 0.5 eV as calculated by B3LYP calculations (see Fig. 6). A similar tautomerism exists also for hydroxy-azoles, i.e., alcohol (R–OH) ⇌ ketone (R=O) or more specifically lactim ⇌ lactam. Also in this case a ketone—an analog of thione—is found to be more stable. In particular, for OH-BimH the difference in stability is about 0.6 eV (Fig. 6). These differences in stability are sufficiently large that these molecules exist almost entirely in thione and ketone tautomeric forms at room temperature. Furthermore, thiones are more stable than thiols also in the adsorbed state [44]. For this reason, only electronic parameters of thione and ketone tautomers are considered in the MEPTIC correlations presented below.

3.4. Evaluation of MEPTIC correlations

In the following we will evaluate if any of the 12 different calculated molecular electronic parameters (p), listed in the technical section (Section 2.2), show any correlation with experimentally determined IE (η). In particular, we test simplistic correlations of the following type:

$$\eta \propto p \quad \text{or} \quad \eta = a + bp, \tag{17}$$

where a and b are fitting parameters. However, we will not limit ourselves to linear correlations, but will instead evaluate if there is any functional dependence between η and p, i.e.:

$$\eta = f(p). \tag{18}$$

It should be noted, however, that we will plot the inhibition efficiency on the abscissa axis and the parameter p on the ordinate axis, because in this way the presentation of data seems somewhat more clear due to the broad range of considered IE and the aspect ratio of the plots.

3.4.1. Evaluation of the whole dataset

Fig. 7 plots the relation between the IE and 12 different molecular electronic parameters. The graphs in the figure are organized into three columns and four rows and in each plot the data points are color symbolized such that the four groups of inhibitors can be differentiated. The range of IE is set the same on all graphs, from −100% to 100%; note that two compounds display IE below −100% (cf. Fig. 4a), hence
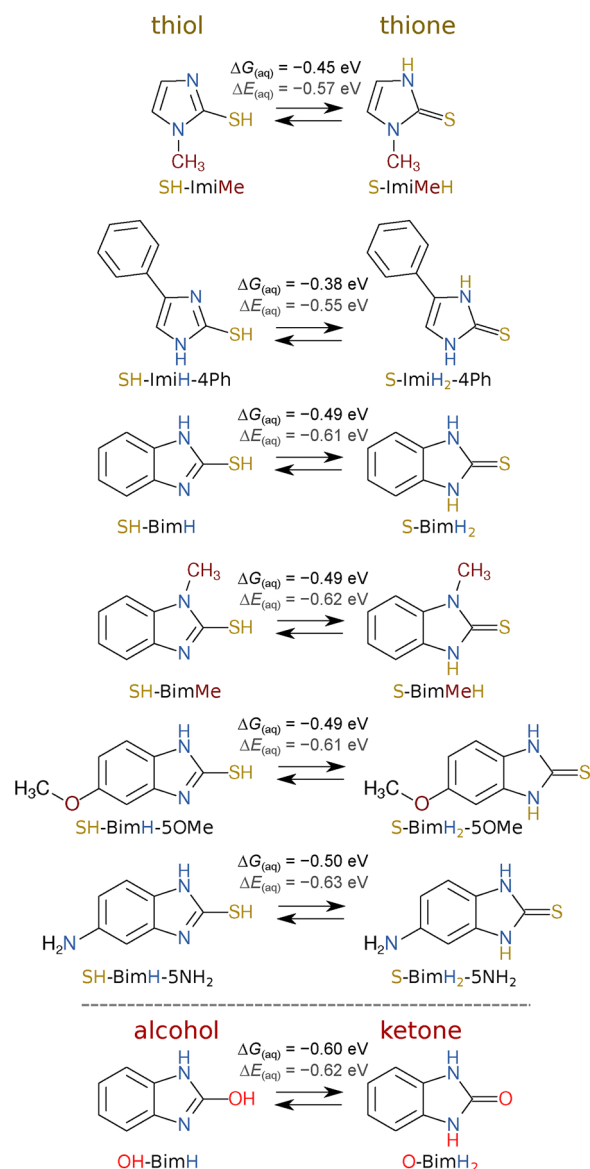

Fig. 6. List of considered mercapto-molecules that can exist in thiol (R–SH, left-side) and thione (R=S, right-side) tautomeric forms, e.g., SH-BimH ⇌ S-BimH₂. A similar alcohol (R–OH, left-side) vs. ketone (R=O, right-side) tautomerism exists also for 2-hydroxybenzimidazole, OH-BimH ⇌ O-BimH₂. According to B3LYP calculations, thiones are by about 0.5 eV more stable than thiols in aqueous solution as indicated by $\Delta G_{(aq)}$, which is the difference between the free energies (at 300 K) of thione and thiol tautomers solvated in implicit water, $\Delta G_{(aq)} = G_{thione(aq)} - G_{thiol(aq)}$ (and analogously for $\Delta E_{(aq)}$). Also for OH-BimH the ketone tautomer is by 0.6 eV more stable than the alcohol tautomer. For isolated molecules in vacuum, the $\Delta G_{(g)}$ and $\Delta E_{(g)}$ values are listed in Table S2 in the Supplementary material.

they fall outside the IE range and are thus not shown. The first (upper) row considers vertical IP, vertical EA, and chemical hardness, calculated by Eqs. (4), (5), and (3), respectively. The second row considers the eigenvalues of HOMO and LUMO as well as the HOMO–LUMO gap. These second row parameters are considered in the vast majority of MEPTIC studies as approximates for IP, EA, and chemical hardness via the relations: $I \approx -\varepsilon_{HOMO}$, $A \approx -\varepsilon_{LUMO}$, and $\eta \approx \frac{1}{2}\Delta\varepsilon$, where η is the chemical hardness (not to be confused with IE, which uses the same symbol in Eqs. (15), (17), and (18)). The third row considers electronegativity (calculated with Eq. (2)), isotropic polarizability, and molecular dipole. The last (fourth) row considers the three important
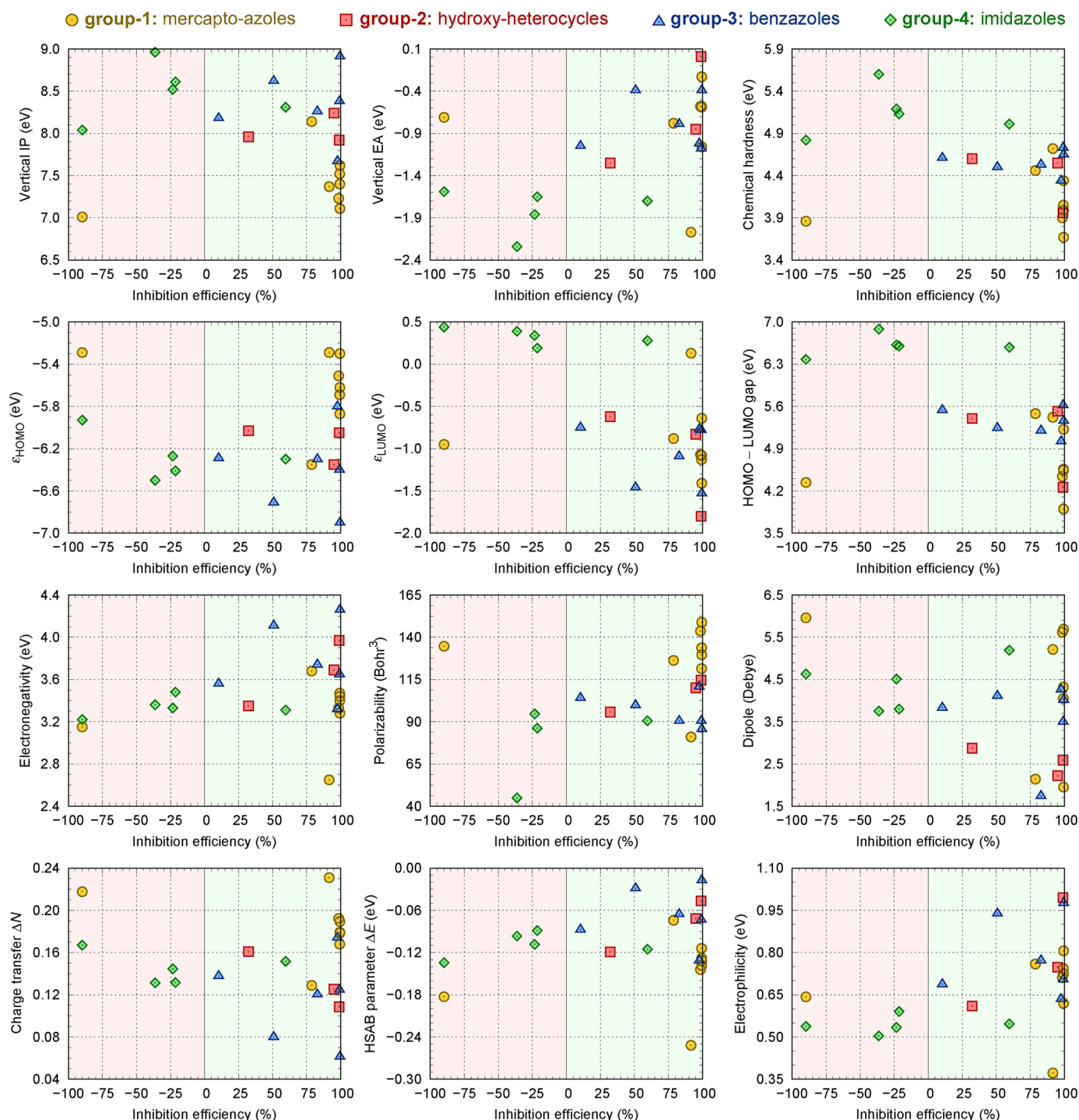
Fig. 7. Correlations (or the lack thereof) between inhibition efficiency and molecular electronic parameters. Notice a large vertical spread of points close to 100% inhibition efficiency for all considered electronic parameters. This indicates that a good inhibitor can display almost any value within a relatively broad range. All molecular electronic parameters are also tabulated in Table S4 in the Supplementary material.

HSAB parameters: charge transfer parameter ΔN and its associated change in energy ΔE as well as electrophilicity index.

Not a single molecular parameter among the twelve considered in Fig. 7 displays any noticeable functional dependence on IE. Instead Fig. 7 reveals a scatter of data points in each of the 12 graphs. In the following, the term "good inhibitor" implies an inhibitor (among the considered compounds) with IE close to 100%. Particularly alarming is the observation of the data points stacked vertically at IE values close to 100%. This implies that there is no correlation between IE and any of the considered parameters, because a good inhibitor can display almost

any value of a given parameter within the considered range, but the considered ranges encapsulate the whole spectrum of molecules from corrosion activators to good inhibitors.

A molecule–surface chemical bond is usually described in terms of a molecule-to-surface donation and a surface-to-molecule back-donation of electron charge [47,48], with a corollary that the larger are the donation and back-donation, the stronger is the molecule–surface bonding. Hence, let us evaluate with the data of Fig. 7 the common inference—nicknamed as "HOMO–LUMO type inference"—that good inhibitors should display (i) a high value of ε_{HOMO} (or low IP) as to favor

molecule-to-surface electron donation, (ii) a low value of ε_{LUMO} (or high EA) as to be able to participate in metal-to-molecule back-donation, and consequently (iii) a small HOMO–LUMO gap (or small chemical hardness).[7] Fig. 7 reveals that good inhibitors display IP in a broad range from about 7 to 9 eV (and $\varepsilon_{HOMO} \in [-6.9, -5.3]$ eV), EA from –1.1 to 0 eV (and $\varepsilon_{LUMO} \in [-1.8, -0.7]$ eV), and chemical hardness from 3.7 to 4.7 eV (and HOMO–LUMO gap from 3.9 to 5.6 eV). These are very broad ranges that extend over 1–2 eV, whereas in the literature it is not uncommon to find the HOMO–LUMO type inferences applied on only two or three inhibitors that show small differences on the order of 0.1 eV. Current results thus make such HOMO–LUMO type inferences dubious at best if not even misleading.

Fig. 7 also shows that, as far as particular values are concerned, the $I \approx -\varepsilon_{HOMO}$ and $A \approx -\varepsilon_{LUMO}$ approximations that are so often used in MEPTIC studies do not hold particularly well, because IP values are by 2 eV larger than $-\varepsilon_{HOMO}$ values and EA is by about the same amount smaller than $-\varepsilon_{LUMO}$ (see also Table S4 in the Supplementary material). However, the trends are much better. This can be most easily seen by comparing the HOMO–LUMO gap plot to that of chemical hardness (note that the latter is calculated rigorously from IP and EA). The two plots show a very similar pattern of data-points scatter. Also the pattern of $-\varepsilon_{HOMO}$ ($-\varepsilon_{LUMO}$) is similar to that of IP (EA), but for visual inspection one needs to flip vertically the ε_{HOMO} and ε_{LUMO} plots.

Electronegativity is another parameter that is often used in MEPTIC studies. Fig. 7, however, reveals that a good inhibitor can display electronegativity over a broad range of values, from 3.3 to 4.3 eV (first graph in the third row), which is a span similar to that discussed above.

Isotropic polarizability (second graph in the third row of Fig. 7) is a parameter which "measures" how easily molecular charge distribution responds to external perturbations. Chemically soft molecules are, in general, more polarizable, hence polarizability is in a sense opposite to chemical hardness. Indeed the trend (or rather the pattern of the data-points scatter) of polarizability is roughly opposite to that of chemically hardness (when comparing the plots, one plot must be vertically flipped), which also indicates that good inhibitors display a broad range of polarizabilities.

The magnitude of the molecular dipole is also often used in MEPTIC studies. It is usually argued that a large dipole is beneficial for corrosion inhibition [49–51], although one can also find the opposite inferences in the literature [52,53]. In contrast, Kokalj argued that the role of the molecular dipole is non-trivial [24]. While arguments based solely on electrostatics indeed show that larger dipole enhances the molecule–surface interaction, the effect on the lateral intermolecular interactions can go both ways, depending on the orientation of molecular dipoles [54]. Fig. 7 reveals that good inhibitors can have a dipole in the range from 1.9 to 5.7 D (the last graph in the third row), but this range encompasses almost all considered molecules.

The last row in Fig. 7 displays the HSAB charge transfer ΔN and its associated change in energy ΔE parameters as well as the electrophilicity index. The ΔN and ΔE parameters were derived by considering the interaction of a Lewis base with a Lewis acid [32] (or a molecule with the metal), whereas the electrophilicity index was derived by considering an electrophilic ligand (or molecule) immersed into an idealized zero-temperature electron gas (reservoir), whose chemical potential is zero [40]. Hence, these three parameters seem to be particularly suited to describe the molecule–surface bonding trends as was indeed verified by several studies [39,55–58]. Nevertheless, Fig. 7 clearly reveals that there is no noticeable correlation between these parameters and IE. Perhaps the assumption that the stronger the inhibitor–surface bonding the better is the inhibitor is not as solid as it seems. This issue will be addressed in a forthcoming publication.

There is a possible objection to the aforementioned argument that

the *data points stacked vertically at IE values close to 100% imply that there is no correlation.* The objection is that if one zooms-in these points—i.e., limits the IE range close to 100%—then perhaps a correlation may appear for only good inhibitors. To address this objection, we provide Fig. 8, which is analogous to Fig. 7, but with the difference that the IE on the abscissa axis is replaced by P_{inh}. To help interpreting Fig. 8, we also provide Fig. 9, which shows how the linear dependence of IE on a parameter (or descriptor) changes if the IE axis is replaced with the P_{inh} axis. Please note that, for compatibility with Figs. 7 and 8, also in Fig. 9 the IE and P_{inh} are represented on abscissa axes. It is clearly evident that none of the 12 plots of Fig. 8 show such dependence as shown in Fig. 9. Furthermore, none of the 12 plots show any clear functional dependence; instead they mainly show a scatter of points. In a very loose terms, one could perhaps say that Fig. 8 suggests that good inhibitors should display low vertical IP and low chemical hardness: by neglecting the outliers there is a loose linear-like dependence of P_{inh} on vertical IP and chemical hardness (or HOMO–LUMO gap). Indeed, that a good inhibitor should display—from qualitative point of view—a relatively low IP and chemical hardness (HOMO–LUMO gap) is reasonable, because a favorable molecule–surface interaction can hardly be expected for a very hard molecule (as an example of hard molecule, let's mention methane). However, the correlation is way too vague to be quantitative, i.e., lower IP or lower chemical hardness (HOMO–LUMO gap) does not in itself imply a better inhibitor. Such a parameter can be instead used as one of descriptors in a machine-learning model as was recently done for inhibitors of Mg corrosion by Feiler et al. [15], who successfully utilized the HOMO–LUMO gap in an artificial neural network model.

3.4.2. Can solvent effects recover the correlations?

Another possible objection to our claim that none among the 12 evaluated molecular electronic parameters correlates with experimentally determined inhibition efficiency is that the apparent lack of correlations is due to neglect of solvation effects (note that electronic descriptors presented in Figs. 7 and 8 refer to isolated molecules in vacuum). However, even if the solvation effects are taken into account (currently with the implicit SMD solvent model [31]), the situation is no better. This is evidenced by Figs. S2 and S3 in the Supplementary material, which are analogous to Figs. 7 and 8, but evaluate the 12 molecular electronic parameters calculated for molecules solvated in implicit water (these parameters are also tabulated in Table S5 in the Supplementary material). Furthermore, molecular solvation energies (Table S3) are also considered therein and Fig. S4 shows that they do not correlate with performance of inhibitors.

3.4.3. Can experimental uncertainties recover the correlations?

Another potential objection to our claim of the lack of correlations is that more techniques should be used to more reliably establish inhibition efficiencies, i.e., the apparent lack of correlations may be due to experimental uncertainties associated with LPR. In this respect, it should be noted that our LPR results do not rely solely on measurements performed at a single immersion time, but were instead accumulated over a 100 h time interval, which was argued to be more reliable [42]. Although some errors in Table S1 appear large, these errors do not critically affect our claim, i.e., as evident from Fig. 4 good inhibitors remain good inhibitors even if the "lower bound" is considered. This is reassuring, because our argument about the lack of correlations is based on good inhibitors, i.e., Fig. 7 clearly reveals they can display almost any value of a given parameter within the range that encompasses the whole spectrum of compounds from corrosion activators to good inhibitors. To further substantiate the reliability of our experimental results, Fig. S5 in the Supplementary material displays potentiodynamic polarization (PDP) curves for several selected cases of good inhibitors and corrosion activators. These PDP curves are clearly coherent with LPR results and confirm the LPR assignments of good inhibitors and corrosion activators.

---

[7] Note that the high value of ε_{HOMO} and the low value of ε_{LUMO} implies the small HOMO–LUMO gap, because $\varepsilon_{HOMO} < \varepsilon_{LUMO}$.
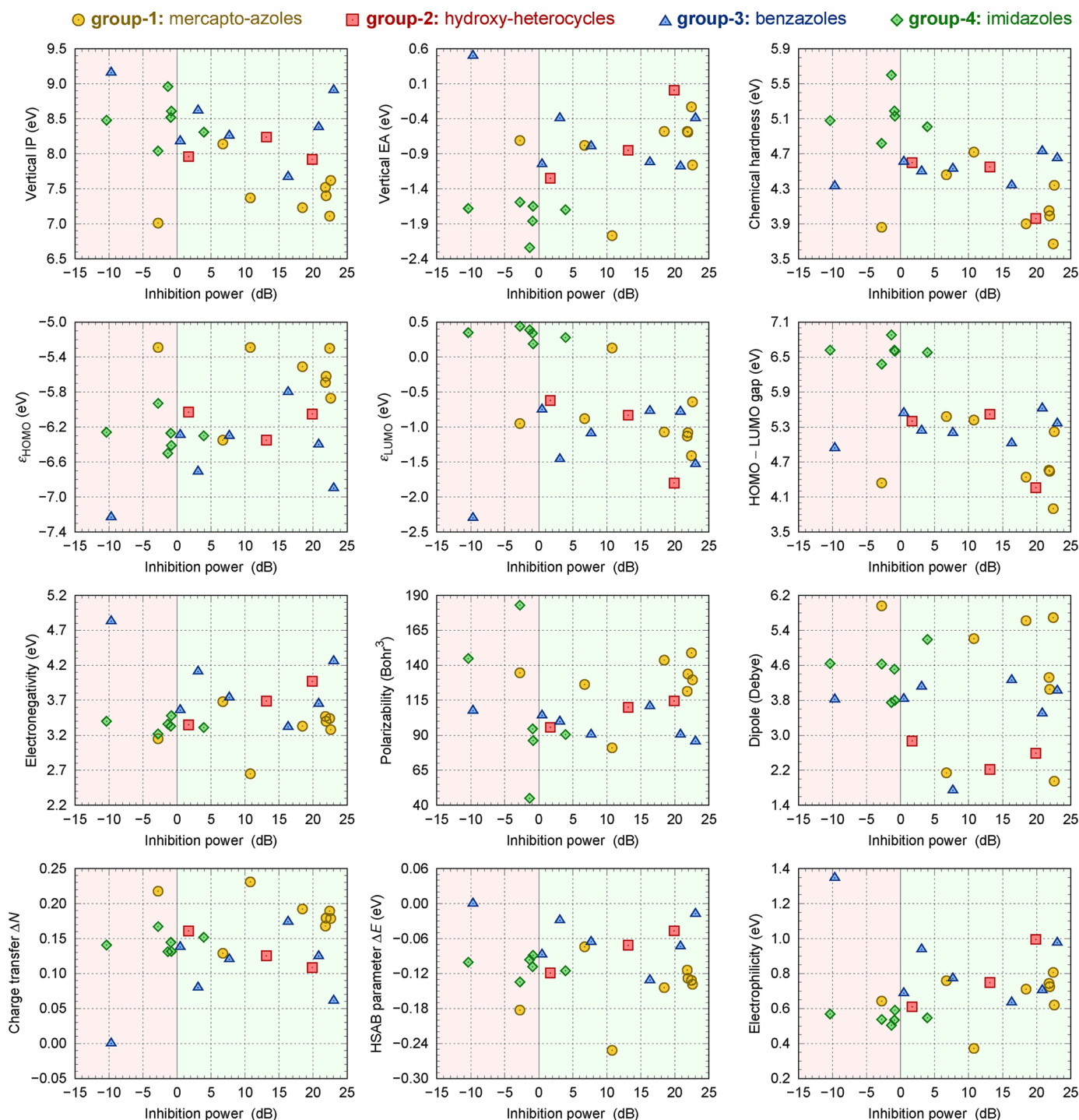
Fig. 8. Similar to Fig. 7, but the inhibition power, $P_{inh} = 10\log_{10}(R_p^{inh}/R_p^{blank})$, is plotted instead of IE on the abscissa axis. Notice the lack of correlation between the performance of inhibitors and their molecular electronic parameters.

3.4.4. Evaluation of individual groups of molecules

Are correlations any better if only a single group of inhibitors is considered? Let us first inspect Fig. 7, which shows parameters vs. IE. The answer is obviously no for mercapto-azoles (yellowish circles), which is the largest group. For benzazoles (blue triangles), there are some linear correlations for HOMO–LUMO gap and polarizability, but only if outliers are discarded. For imidazoles (green diamonds) a linear correlation appears for ε_{LUMO} if two outliers are discarded (both are activators and one of them is not shown as it falls outside the shown IE range). As for hydroxy-heterocycles (red squares), polarizability and to lesser extent ΔN and ΔE correlate with IE, but beware that there are

only three corresponding data points. Now let us consider Fig. 8, which shows parameters vs. P_{inh}. In this figure the only obvious correlations are for hydroxy-molecules (for EA, chemical hardness, electronegativity, polarizability, ΔN, ΔE, and electrophilicity), but beware that there are only three corresponding data points. The bottom line of this inspection is that for a small number of points, one may find correlations, but the correlations disappear for larger number of points. This hints at a chance correlation for small number of points. Furthermore, it is possible for many plots shown in Figs. 7 and 8 to find nice linear correlations by cherry-picking only a subset of points (unfortunately, many of us have, at least unintentionally, a tendency to
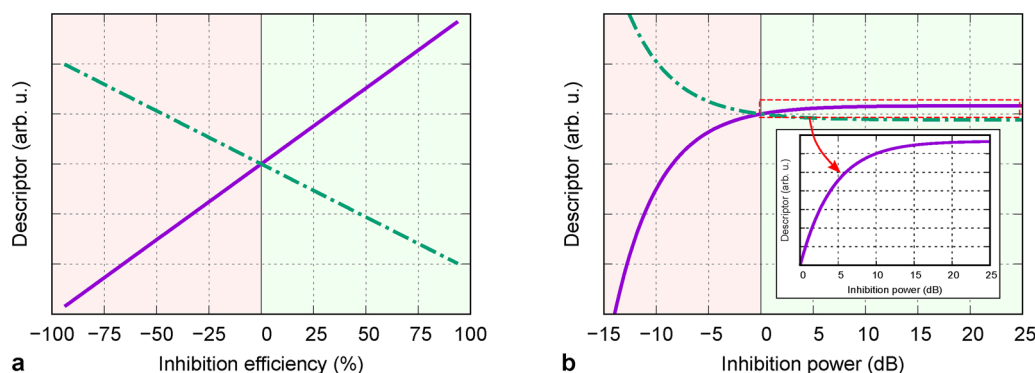
Fig. 9. (a) If a descriptor shows a linear dependence on IE, then (b) shows the corresponding dependence for a descriptor plotted as a function of inhibition power, $P_{inh} = 10\log_{10}(R_p^{inh}/R_p^{blank})$. Purple and green curves represent respectively the correlation and anticorrelation between the descriptor and IE. The ranges of IE and P_{inh} are set compatible to Figs. 7 and 8, respectively. Note that $P_{inh} \in [-15\,dB, 25\,dB]$ corresponds to IE $\in [-3000\%, 99.7\%]$. The inset of (b) is a zoom-in and shows the dependence of the purple curve for positive range of P_{inh}. (For interpretation of the references to color in this figure legend, the reader is referred to the web version of this article.)

cherry-pick). This last fact together with chance correlations, mentioned above, should be kept in mind when a MEPTIC type correlation is claimed for a small number of data points.

4. Conclusion

In summary, we showed that none among the evaluated molecular electronic parameters (ionization potential, electron affinity, chemical hardness, electronegativity, HOMO and LUMO eigenvalues, HOMO–LUMO gap, polarizability, dipole, HSAB ΔN and ΔE parameters, electrophilicity, and solvation energies) correlates with experimentally determined inhibition efficiency for a set of 24 heterocyclic organic compounds, tested as corrosion inhibitors for copper in 3 wt.% NaCl aqueous solution. While this is a negative result, we believe it is very important, because the literature is replete with studies, based on only a few inhibitors, where purported correlations between such parameters and inhibition efficiency are claimed. Our analysis indeed demonstrates that it is possible to find such correlations by narrowing down the number of molecules (or by cherry-picking) thus considering only a few similar molecules, however, such correlations are susceptible to chance correlation and even more so to spurious correlation fallacy. This fact should be kept in mind when a MEPTIC type correlation is claimed for a small number of data points.

Our study therefore strongly suggests that a simple MEPTIC approach is not apt. We therefore appeal to the community that the practice where a MEPTIC type correlation is claimed for a small number of inhibitors should cease. Instead, focus should be given to more appropriate approaches. Among them, machine-learning (ML) techniques seem to currently have the largest potential to generate reasonably robust and predictive models for screening new inhibitors, however, the challenge is to provide adequate descriptors, because descriptors affect the quality of the ML models much more than the ML algorithm does [16]. Although ML techniques have the capacity to find the otherwise hidden correlations, they will not reveal the underlying reasons for them, and thus, ML algorithms may mostly serve as a test-bench for newly proposed inhibitor descriptors and *in silico* trial-and-error screening of new inhibitors. We therefore believe that the search for physically sound descriptors and their integration into an appropriate model is the key and in this context explicit modeling of interactions between components of corrosion system and their dynamics have the potential to provide them.

Finally, we also elucidated the nonlinearity problem of the often used inhibition efficiency metric and introduced a new metric for evaluating the performance of corrosion inhibitors, termed *inhibition power*, that uses the logarithmic scale and dimensionless decibel (dB) units. The new metric is not susceptible to the nonlinearity problem.

Author contributions

Anton Kokalj: Conceptualization, methodology, investigation, formal analysis, writing – original draft, writing – reviewing and editing, visualization, funding acquisition, supervision, project administration. Matic Lozinšek: Conceptualization, investigation, writing – reviewing and editing. Barbara Kapun: Conceptualization, investigation. Peyman Taheri: Conceptualization. Shova Neupane: Conceptualization. Patricia Losada-Pérez: Conceptualization. Chenyang Xie: Conceptualization. Stojan Stavber: Conceptualization. Daniel Crespo: Conceptualization, methodology, writing – reviewing and editing, funding acquisition. Frank U. Renner: Conceptualization, funding acquisition. Arjan Mol: Conceptualization, methodology, funding acquisition. Ingrid Milošev: Conceptualization, methodology, investigation, supervision.

Conflict of interest

The authors declare that there is no conflict of interest.

Appendix A. Supplementary data

Supplementary data associated with this article can be found, in the online version, at https://doi.org/10.1016/j.corsci.2020.108856.

References

[1] T.G. Harvey, S.G. Hardin, A.E. Hughes, T.H. Muster, P.A. White, T.A. Markley, P.A. Corrigan, J. Mardel, S.J. Garcia, J.M.C. Mol, A.M. Glenn, The effect of inhibitor structure on the corrosion of AA2024 and AA7075, Corros. Sci. 53 (2011) 2184–2190.

[2] P.A. White, G.B. Smith, T.G. Harvey, P.A. Corrigan, M.A. Glenn, D. Lau, S.G. Hardin, J. Mardel, T.A. Markley, T.H. Muster, N. Sherman, S.J. Garcia, J.M.C. Mol, A.E. Hughes, A new high-throughput method for corrosion testing, Corros. Sci. 58 (2012) 327–331.

[3] D.A. Winkler, M. Breedon, A.E. Hughes, F.R. Burden, A.S. Barnard, T.G. Harvey, I. Cole, Towards chromate-free corrosion inhibitors: structure-property models for organic alternatives, Green Chem. 16 (2014) 3349–3357.

[4] S.V. Lamaka, B. Vaghefinazari, D. Mei, R.P. Petrauskas, D. Höche, M.L. Zheludkevich, Comprehensive screening of Mg corrosion inhibitors, Corros. Sci. 128 (2017) 224–240.

[5] B.D. Chambers, S.R. Taylor, M.W. Kendig, Rapid discovery of corrosion inhibitors and synergistic combinations using high-throughput screening methods, Corrosion 61 (2005) 480–489.

[6] T.H. Muster, A.E. Hughes, S.A. Furman, T. Harvey, N. Sherman, S. Hardin, P. Corrigan, D. Lau, F.H. Scholes, P.A. White, M. Glenn, J. Mardel, S.J. Garcia, J.M.C. Mol, A rapid screening multi-electrode method for the evaluation of corrosion inhibitors, Electrochim. Acta 54 (2009) 3402–3411.

[7] T.H. Muster, A. Trinchi, T.A. Markley, D. Lau, P. Martin, A. Bradbury, A. Bendavid, S. Dligatch, A review of high throughput and combinatorial electrochemistry, Electrochim. Acta 56 (2011) 9679–9699.

[8] I.S. Cole, A.E. Hughes, Designing molecular protection: new paradigm for developing corrosion resistant materials uniting high throughput studies, multiscale modelling and self-repair, Corros. Eng. Sci. Technol. 49 (2014) 109–115.

[9] T. Würger, C. Feiler, F. Musil, G.B.V. Feldbauer, D. Höche, S.V. Lamaka, M.L. Zheludkevich, R.H. Meißner, Data science based Mg corrosion engineering, Front. Mater. 6 (2019) 53.

[10] G. Gece, The use of quantum chemical methods in corrosion inhibitor studies, Corros. Sci. 50 (2008) 2981–2992.

[11] I.B. Obot, T.D. Macdonald, Z.M. Gasem, Density functional theory (DFT) as a powerful tool for designing new organic corrosion inhibitors. Part 1: an overview, Corros. Sci. 99 (2015) 1–30.

[12] A. Kokalj, D. Costa, Molecular modeling of corrosion inhibitors, in: K. Wandelt (Ed.), Encyclopedia of Interfacial Chemistry, Elsevier, 2018, pp. 332–345 , https://doi.org/10.1016/B978-0-12-409547-2.13444-4.

[13] H. Ke, C.D. Taylor, Density functional theory: an essential partner in the integrated computational materials engineering approach to corrosion, Corrosion 75 (2019) 708–726.

[14] D.A. Winkler, M. Breedon, P. White, A.E. Hughes, E.D. Sapper, I. Cole, Using high throughput experimental data and *in silico* models to discover alternatives to toxic chromate corrosion inhibitors, Corros. Sci. 106 (2016) 229–235.

[15] C. Feiler, D. Mei, B. Vaghefinazari, T. Würger, R.H. Meißner, B.J.C. Luthringer-Feyerabend, D.A. Winkler, M.L. Zheludkevich, S.V. Lamaka, *In silico* screening of modulators of magnesium dissolution, Corros. Sci. 163 (2020) 108245.

[16] T.L.P. Galvão, G. Novell-Leruth, A. Kuznetsova, J. Tedim, J.R.B. Gomes, Elucidating structure–property relationships in aluminum alloy corrosion inhibitors by machine learning, J. Phys. Chem. C 124 (2020) 5624–5635.

[17] C.T. Ser, P. Žuvela, M.W. Wong, Prediction of corrosion inhibition efficiency of pyridines and quinolines on an iron surface using machine learning-powered quantitative structure-property relationships, Appl. Surf. Sci. 512 (2020) 145612.

[18] L. Li, X. Zhang, S. Gong, H. Zhao, Y. Bai, Q. Li, L. Ji, The discussion of descriptors for the QSAR model and molecular dynamics simulation of benzimidazole derivatives as corrosion inhibitors, Corros. Sci. 99 (2015) 76–88.

[19] M.H. Keshavarz, K. Esmaeilpour, A.N. Golikand, Z. Shirazi, Simple approach to predict corrosion inhibition efficiency of imidazole and benzimidazole derivatives as well as linear organic compounds containing several polar functional groups, Z. Anorg. Allg. Chem. 642 (2016) 906–913.

[20] A.M. Al-Fakih, Z.Y. Algamal, M.H. Lee, H.H. Abdallah, H. Maarof, M. Aziz, Quantitative structure-activity relationship model for prediction study of corrosion inhibition efficiency using two-stage sparse multiple linear regression, J. Chemom. 30 (2016) 361–368.

[21] Y. Liu, Y. Guo, W. Wu, Y. Xiong, C. Sun, L. Yuan, M. Li, A machine learning-based QSAR model for benzimidazole derivatives as corrosion inhibitors by incorporating comprehensive feature selection, Interdiscip. Sci.: Comput. Life Sci. 11 (2019) 738–747.

[22] D.A. Winkler, Predicting the performance of organic corrosion inhibitors, Metals 7 (2017) 553.

[23] J.O'M. Bockris, A.K.N. Reddy, 2nd ed., Modern Electrochemistry Vol. 2B Kluwer Academic/Plenum Publishers, New York, 2000.

[24] A. Kokalj, Is the analysis of molecular electronic structure of corrosion inhibitors sufficient to predict the trend of their inhibition performance, Electrochim. Acta 56 (2010) 745–755.

[25] A. Kokalj, S. Peljhan, M. Finšgar, I. Milošev, What determines the inhibition effectiveness of ATA, BTAH, and BTAOH corrosion inhibitors on copper? J. Am. Chem. Soc. 132 (2010) 16657–16668.

[26] P. Morales-Gil, M.S. Walczak, R.A. Cottis, J.M. Romero, R. Lindsay, Corrosion inhibitor binding in an acidic medium: interaction of 2-mercaptobenizmidazole with carbon-steel in hydrochloric acid, Corros. Sci. 85 (2014) 109–114.

[27] M.J. Frisch, G.W. Trucks, H.B. Schlegel, G.E. Scuseria, M.A. Robb, J.R. Cheeseman, G. Scalmani, V. Barone, G.A. Petersson, H. Nakatsuji, X. Li, M. Caricato, A.V. Marenich, J. Bloino, B.G. Janesko, R. Gomperts, B. Mennucci, H.P. Hratchian, J.V. Ortiz, A.F. Izmaylov, J.L. Sonnenberg, D. Williams-Young, F. Ding, F. Lipparini,
F. Egidi, J. Goings, B. Peng, A. Petrone, T. Henderson, D. Ranasinghe, V.G. Zakrzewski, J. Gao, N. Rega, G. Zheng, W. Liang, M. Hada, M. Ehara, K. Toyota, R. Fukuda, J. Hasegawa, M. Ishida, T. Nakajima, Y. Honda, O. Kitao, H. Nakai, T. Vreven, K. Throssell, J.A. Montgomery Jr., J.E. Peralta, F. Ogliaro, M.J. Bearpark, J.J. Heyd, E.N. Brothers, K.N. Kudin, V.N. Staroverov, T.A. Keith, R. Kobayashi, J. Normand, K. Raghavachari, A.P. Rendell, J.C. Burant, S.S. Iyengar, J. Tomasi, M. Cossi, J.M. Millam, M. Klene, C. Adamo, R. Cammi, J.W. Ochterski, R.L. Martin, K. Morokuma, O. Farkas, J.B. Foresman, D.J. Fox, Gaussian 16 Revision A.03, Gaussian Inc., Wallingford, CT, 2016.

[28] A.D. Becke, Density-functional thermochemistry. III. The role of exact exchange, J. Chem. Phys. 98 (1993) 5648–5652.

[29] S.F. Sousa, P.A. Fernandes, M.J. Ramos, General performance of density functionals, J. Phys. Chem. A 111 (2007) 10439–10452.

[30] F. Weigend, R. Ahlrichs, Balanced basis sets of split valence, triple zeta valence and quadruple zeta valence quality for H to Rn: design and assessment of accuracy, Phys. Chem. Chem. Phys. 7 (2005) 3297–3305.

[31] A.V. Marenich, C.J. Cramer, D.G. Truhlar, Universal solvation model based on solute electron density and on a continuum model of the solvent defined by the bulk dielectric constant and atomic surface tensions, J. Phys. Chem. B 113 (2009) 6378–6396.

[32] R.G. Parr, R.G. Pearson, Absolute hardness: companion parameter to absolute electronegativity, J. Am. Chem. Soc. 105 (1983) 7512–7516.

[33] R.G. Pearson, Hard and soft acids and bases, J. Am. Chem. Soc. 85 (1963) 3533–3539.

[34] J.P. Perdew, R.G. Parr, M. Levy, J.L. Balduz Jr., Density-functional theory for fractional particle number: derivative discontinuities of the energy, Phys. Rev. Lett. 49 (1982) 1691–1694.

[35] R.G. Parr, W. Yang, Density-Functional Theory of Atoms and Molecules, Oxford University Press, Inc., New York, 1989.

[36] R.G. Parr, R.A. Donnelly, M. Levy, W.E. Palke, Electronegativity: the density functional viewpoint, J. Chem. Phys. 68 (1978) 3801–3807.

[37] R.P. Iczkowski, J.L. Margrave, Electronegativity, J. Am. Chem. Soc. 83 (1961) 3547–3551.

[38] R.G. Pearson, The HSAB principle — more quantitative aspects, Inorg. Chim. Acta 240 (1995) 93–98.

[39] A. Kokalj, On the HSAB based estimate of charge transfer between adsorbates and metal surfaces, Chem. Phys. 393 (2012) 1–12.

[40] R.G. Parr, L.v. Szentpály, S. Liu, Electrophilicity index, J. Am. Chem. Soc. 121 (1999) 1922–1924.

[41] A. Kokalj, N. Kovačević, On the consistent use of electrophilicity index and HSAB-based electron transfer and its associated change of energy parameters, Chem. Phys. Lett. 507 (2011) 181–184.

[42] P. Taheri, I. Milošev, M. Meeusen, B. Kapun, P. White, A. Kokalj, A. Mol, On the importance of time-resolved electrochemical evaluation in corrosion inhibitor-screening studies, npj Mater. Degrad. 4 (2020) 12, https://doi.org/10.1038/s41529-020-0116-z.

[43] G.R. Form, E.S. Raper, T.C. Downie, The crystal and molecular structure of 2-mercaptobenzimidazole, Acta Crystallogr. B 32 (1976) 345–348.

[44] N. Kovačević, I. Milošev, A. Kokalj, The roles of mercapto, benzene, and methyl groups in the corrosion inhibition of imidazoles on copper: II. Inhibitor–copper bonding, Corros. Sci. 98 (2015) 457–470.

[45] N. Biswas, S. Thomas, A. Sarkar, T. Mukherjee, S. Kapoor, Adsorption of methimazole on silver nanoparticles: FTIR, Raman, and surface-enhanced Raman scattering study aided by density functional theory, J. Phys. Chem. C 113 (2009) 7091–7100.

[46] G. Liu, H. Zeng, Q. Lu, H. Zhong, P. Choi, Z. Xu, Adsorption of mercaptobenzoheterocyclic compounds on sulfide mineral surfaces: a density functional theory study of structure-reactivity relations, Colloids Surf. A 409 (2012) 1–9.

[47] R. Hoffmann, A chemical and theoretical way to look at bonding on surfaces, Rev. Mod. Phys. 60 (1988) 601–628, https://doi.org/10.1103/RevModPhys.60.601.

[48] B. Hammer, J.K. Nørskov, Theoretical surface science and catalysis — calculations and concepts, Adv. Catal. 45 (2000) 71–129.

[49] M. Şahin, G. Gece, F. Karcı, S. Bilgiç, Experimental and theoretical study of the effect of some heterocyclic compounds on the corrosion of low carbon steel in 3.5% NaCl medium, J. Appl. Electrochem. 38 (2008) 809–815.

[50] I.B. Obot, N.O. Obi-Egbedi, Theoretical study of benzimidazole and its derivatives and their potential activity as corrosion inhibitors, Corros. Sci. 52 (2010) 657–660.

[51] A. Stoyanova, G. Petkova, S.D. Peyerimhoff, Correlation between the molecular structure and the corrosion inhibiting effect of some pyrophthalone compounds, Chem. Phys. 279 (2002) 1–6.

[52] N. Khalil, Quantum chemical approach of corrosion inhibition, Electrochim. Acta 48 (2003) 2635–2640.

[53] G. Gao, C. Liang, Electrochemical and DFT studies of β-amino-alcohols as corrosion inhibitors for brass, Electrochim. Acta 52 (2007) 4554–4559.

[54] A. Kokalj, Electrostatic model for treating long-range lateral interactions between polar molecules adsorbed on metal surfaces, Phys. Rev. B 84 (2011) 045418.

[55] N. Kovačević, A. Kokalj, DFT study of interaction of azoles with Cu(111) and Al (111) surfaces: role of azole nitrogen atoms and dipole–dipole interactions, J. Phys. Chem. C 115 (2011) 24189–24197.

[56] N. Kovačević, A. Kokalj, The relation between adsorption bonding and corrosion inhibition of azole molecules on copper, Corros. Sci. 73 (2013) 7–17.

[57] P. Crawford, P. Hu, Reactivity of the 4d transition metals toward N hydrogenation and NH dissociation: a DFT-based HSAB analysis, J. Phys. Chem. B 110 (2006) 4157–4161.

[58] P. Crawford, P. Hu, Importance of electronegativity differences and surface structure in molecular dissociation reactions at transition metal surfaces, J. Phys. Chem. B 110 (2006) 24929–24935.